1

Visual Perception of Semi-transparent Blotches: Detection and Restoration

V. Bruni[1], A. J. Crawford[1], A. Kokaram[2] and D. Vitulano[1]
[1]*Istituto per le Applicazioni del Calcolo "M. Picone"- C.N.R.*
[2]*Electronic and Electrical Engineering Department, University of Dublin, Trinity College*
[1]*Italy*, [2]*Ireland*

1. Introduction

Digital image restoration has become a popular area of research (Gonzalez & Woods,2002). The increased demand for archived material and the increasing power of computers have led to a need for digital methods for the restoration of degradation. Common degradation includes noise, line-scratches, tear, moire, shake and flicker (see for instance (Bruni & Vitulano, 2004; Corrigan & Kokaram, 2004; Kokaram, 1998; Kokaram, 2004; Roosmalen et al., 1999)).

An important area in digital image processing, and in particular in digital restoration, is human visual perception (Winkler, 2005). Perception laws are crucial in several image processing models. They allow for the improvement of the visual quality of the result using adaptive and automatic methods. The visibility of a given object over a background depends on contrast sensitivity, luminance adaptation and contrast masking (Winkler, 2005; Damera-Venkata et al,2000; Gutiérrez et al., 2006; Barba & Barba, 2002; Pappas & Safranek, 2000). These measures are well defined for uniform objects over uniform backgrounds while they may fail in presence of sinusoidal stimuli, i.e. highly detailed regions (Damera-Venkata et al,2000; Nadenau et al., 2003). In this case, perception depends on the distance between the observer and the object, according to the width of the analysed region and the frequency of the stimulus. It turns out that point-wise contrast measures that do not take into account the global visibility of an object in a given image, can fail in the presence of complicated patterns.

Figure 1. Examples of semi-transparent blotches: Note the variation in intensity and colour while the underlying detail remains

This is the case for semi-transparent blotches which partially or completely obscure regions of images (see Fig. 1). They are usually caused by dirt or moisture on archived material and can be seen as complicated objects over more or less detailed patterns (Kokaram, 1998; Stanco et al. 2005). They appear as irregular regions with variable shape and size, having a slightly different colour from the original one. This is the reason why they can be easily confused with scene components. The additional difficulty is their semi-transparency since they do not completely hide the underlying original information. Classical restoration or inpainting methods (Gonzalez & Woods, 2002; Bertalmio et al. 2000; Criminisi et al. 2004) cannot be used as the original image content must be retained: this is an important issue from an historical point of view. It turns out that their recognition and restoration require the introduction of global measures, like the contrast of a region (group of pixels), instead of pixel-wise measures.

This chapter introduces a generalized perception based model that mainly exploits two global perception based measures oriented to the detection of the most visible object over a given context. In order to be significant, they must be evaluated over an image component (frequency, colour channel, etc.) where the blotches are more visible --- often the most visible part. This component is used both for detecting and for modelling the overall blotch shape. This is then used to guide the blotch removal in the remaining image components according to human perception. The choice of the best component can be inferred by the physical model that causes the degradation under study. The distortion measures account for the variation of the visibility of a set of pixels over a changing background and the variation of the visibility of a changing set of pixels over a fixed background. The 'changing' function can be modified with respect to the analysed case. In the simplest case the clipping operator can be used. Its aim is to separate two different regions, as is the case for the detection and restoration of semi-transparent blotches. The two measures are based on the hypothesis that blotches are detectable (by human observers) at a 'first glance' over the image, since they are recognized as "foreign" objects in different contexts over the same image. The two measures can be used for both a global detection and a local refinement of the result: the largest region where the blotch is the most visible object. The proposed approach has been tested on two very frequent examples: scratches on old films (Kokaram, 1998) and water blotches on archived documents (Stanco et al., 2005). Extensive experimental results have shown that the proposed model achieves high visual quality results in very delicate situations, in a completely automatic manner and with a low computational effort.

2. A perception based model

As already discussed in the previous section, semi-transparent blotches are very difficult to manage because of their structure: they show the same frequency properties of the affected image. Nonetheless, they are usually perceived by a human observer 'at first glance'. It is very difficult to understand the mechanics of this process because of the high variability of both the blotch appearance and the image context of the blotch. In fact, if on one hand their intrinsic structure produces a sort of masking, on the other this peculiarity enhances its visual detection by a human observer. The proposed model tries to exploit this contradictory aspect in order to write a mathematical model that may fit this very singular behaviour.

Figure 2. Original Pyramid image (*Left*) and its Saturation component (*Right*): blotches are more visible in the Saturation component and appear as bright regions

The model may be synthesized as follows. A degraded image I has to be projected, via an operator Π, into a new space where semi-transparent blotches become the most visible object in the scene. This step tries to simulate the human visual system that reacts in presence of this kind of defect. Π's structure will depend on both the physical model that produced the blotch and the resolution (or equivalently the scale) r at which the blotch shows its greatest visibility. Once the operator Π has been performed, a distortion measure that accounts for the visibility of the blotch has to be introduced. As already outlined, available contrast definitions generally account for pixel-wise measures. Moreover, an (opaque) object over a uniform or regular background is usually considered. But this is not our case: the blotch under investigation does not completely cover the background and very often preserves and inherits the background characteristics. In the following a new distortion DET that will account for this requirement will be introduced. The cascade of the two aforementioned operators completes the first phase whose objective is an automatic detection of the blotch. In order to achieve a restored image, the output of the cascade above will be the input of the restoration operator RES. It will depend, again, on the physical model that produced the blotch. Here this dependence plays a fundamental role, since it gives the 'a priori' knowledge that makes this phase somewhat independent of the context, and therefore, of the underlying image. It is obvious that the deeper the knowledge about the formation of degradation, the lower the dependence of the restoration on the original image. This aspect gives a noticeable advantage with respect to other classical image processing problems like, for instance, denoising. It is worth outlining the fact that the operator RES is not necessarily defined in the space produced by Π but also in its complementary (not necessarily orthogonal) one. Mathematically speaking, the detection phase can be written:

$$DET(\Pi(I), r, p) = B_{mask} \tag{1}$$

where the symbols have already been introduced apart from p that indicates the prior knowledge about the physical model producing the blotch. The restoration phase, then, results:

$$RES(B_{mask}, \Pi(I), p, r) = \hat{I} \tag{2}$$

where $\hat{I}$ is the restored image.

3. Optimal space for vision

The first step consists of introducing a suitable operator Π that projects the image I in a space that allows an improved detection. Such an operator can be built only with a deep knowledge of the physical process that generates the blotch. That is why this operation is probably the most delicate part of the whole detection process. It corresponds to a combination of two well known tasks in image processing: features extraction and image enhancement (Gonzalez & Woods, 2002). For instance, for particular blotches like those caused by the contact between water and paper, a possible space may be the saturation component in the HSV colour space, as shown in Fig. 2. The interesting aspect to outline is that this operation is not unique. In fact, in some cases the appearance of the blotch may present more than one peculiarity, such as luminance regularity or a particular colour. Hence, the projection operator can exploit just some or all of these characteristics to determine the best projection space. For this reason, the projection operator can also be enriched by further features that better characterize the blotch.

3.1 Optimal scale for perception

Even though blotches are usually non-homogeneous, they are perceived as uniform areas since the complex background masks its coarseness. A low pass filter simulates this effect: it removes the redundant frequencies that are not perceived by the HVS and therefore enhances those regions that are perceived as homogeneous. Key to this phase is to select the optimum level of resolution $\bar{r}$. It must be a good trade off between the enhancement of the degraded region, the preservation of the geometrical shape and location of the blotch. $\bar{r}$ can be automatically selected by computing the contrast between two successive low-pass filtered versions of the detection space. A moving average filter ϕ of size r can be then used to smooth the output Π(I) of the projection operator. The definition of contrast given by Peli (Peli, 1990) can be employed.

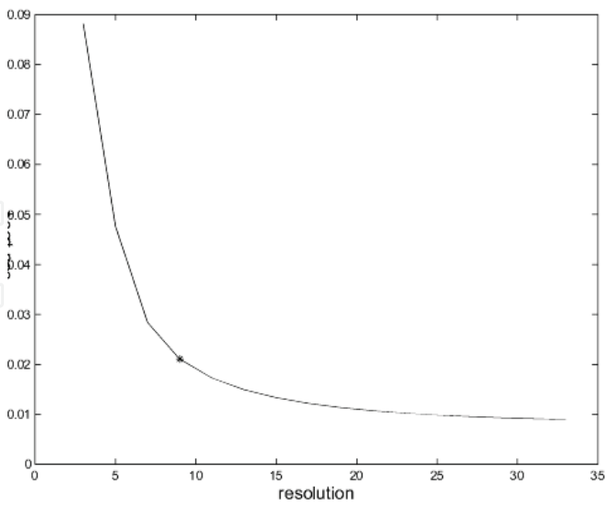

Figure 3. A typical contrast curve $C(r)$ (eq. (3)) versus resolution r. The star indicates the point where the contrast becomes less than Weber's threshold (0.02)

The rationale is that the best level of resolution $\bar{r}$ is that which measures the minimum perceivable contrast (i.e. 0.02) between two successive blurred images, i.e.

$$C(r) = \frac{1}{|\Omega|} \sum_{(x,y)\in\Omega} \frac{\left|(\Pi(I) * \phi_r)(x,y) - (\Pi(I) * \phi_{r-1})(x,y)\right|}{(\Pi(I) * \phi_r)(x,y)}, \tag{3}$$

where Ω is the image domain and $|\Omega|$ is its size. A typical behaviour of the contrast curve versus the level of resolution is depicted in Fig. 3. It is a decreasing function and the optimal point $\bar{r}$ coincides with the maximum inflection of the curve.

3.2 Contrast measures for detection

The major contribution of this part is the introduction of two new distortion measures. Their combination accounts for the global blotch visibility in the whole remaining image. Degraded regions are selected from the image $\Pi_{\bar{r}}(I)$ coming from the projection operator at the optimal scale, as shown above, i.e. $\Pi_{\bar{r}}(I) = \Pi(I) * \phi_{\bar{r}}$. A clipping operation with a perception based threshold value is then performed and a distortion measure is evaluated. The distortion metric accounts for the fact that non-uniform regions can be perceived as homogeneous. Thanks to the introduced distortion, clipping extracts the most visible regions by automatically selecting the correct threshold.

In particular, successive thresholds are applied to $\Pi_{\bar{r}}(I)$. They give different distortion values, whose maximum is achieved in correspondence to the most visible regions.

The clipping operator Θ is defined as follows:

$$\Theta(\Pi_{\bar{r}}(I), Th(t)) = \begin{cases} \Pi_{\bar{r}}(I) & \text{if} \quad \Pi_{\bar{r}}(I)(x,y) \le Th(t) \\ Th(t) & \text{otherwise} \end{cases} \tag{4}$$

The threshold value $Th(t) \in [L_{\min}, L_{\max}]$, where $L_{\min}$ and $L_{\max}$ are the minimum and maximum admissible values for *Th*, i.e.

$$Th(t) = L_{\min} + t\ \Delta t \tag{5}$$

t is the time variable (*t*=0,1,2,...) while Δ*t* is the time unit.

The distortion caused by the clipping operation can be defined as follows:

$$D(\Omega_t) = \frac{1}{|\Omega_t|} \sum_{(x,y)\in\Omega_t} D_1(x,y) D_2(x,y) \tag{6}$$

where Ω_t is the size of the region of the current blotch — i.e. detected through the actual threshold value Th(t). The first measure $D_1(x,y)$, gives the perceived distortion as the average contrast between the clipped regions of $\Pi_{\bar{r}}(I)$ and the clipping threshold value $Th(t)$ and it is defined as:

$$D_1(x,y) = \frac{\Pi_{\bar{r}}(I)(x,y) - Th(t)}{M}, \qquad \forall (x,y) \in \Omega_t \tag{7}$$

It measures the change in perception between the image with respect to the fixed background *M* (i.e. the mean of the degraded image), before and after clipping. In other words, it evaluates how an object of intensity $\Pi_{\bar{r}}(I)$ changes if it is substituted for the

threshold value $Th(t)$. $D_1(x,y)$ is a decreasing function whose shape is depicted in Fig. 4 (left). Initially, for a decreasing threshold, it grows quickly as the clipping involves non-uniform regions with small areas. Subsequently, points with values close to the background are selected and the behaviour changes, as the threshold approaches M.

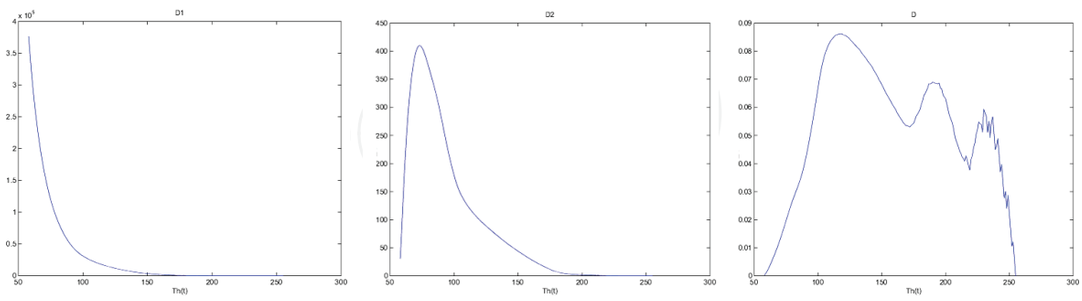

Figure 4. Distortion Curves for Pyramid image: Shown above are plot of the Distortion D_1 (Left), D_2 (Middle) and the total distortion D (Right) (using, $L_{\min} = M$, $L_{\max} = 255$ and Δt=1)

The distortion D_2 measures the change of the contrast of the same object $\Pi_{\bar{r}}(I)$ over different backgrounds (M_t and M):

$$D_2(x,y) = \frac{\Pi_{\bar{r}}(I)(x,y)(M_t - M)}{M_t M}, \qquad \forall (x,y) \in \Omega_t \tag{8}$$

Note that M_t is the background of the image after the clipping operation. It will be different from the initial M of the unclipped (original) degraded image. D_2 is the product of two different components: the first, $\Pi_{\bar{r}}(I)/\ M_t$, is a growing function with respect to the time t, i.e. as M_t decreases. The second, $(M_t - M)/M$, is a decreasing function converging to zero. As Fig. 4 (middle) shows, for larger threshold values, the term $(M_t - M)/M$ gives a minor contribution as the clipping operator selects few pixels and M_t does not change significantly. However, as the threshold decreases, M_t approaches M faster as more points close to the background are selected. Therefore, D_2 approaches zero for lower threshold values.
Combining D_1 and D_2, the maximum global distortion gives the detection threshold (see Fig. 4 (right)). As it can be observed, the distortion D achieves a trade off between the foreground and the background of the image at its maximum value. It represents the maximum contrast for the image, i.e. the maximum allowed distortion, which is able to separate different objects of the image without introducing artifacts. In fact, from that point on, pixels of the background are selected by the clipping operator, mixing the degradation and the original image. It is worth outlining that has been made the assumption that blotches are the brighter parts of the image $\Pi_{\bar{r}}(I)$. The blotch mask is found as all pixels greater than $Th(t_{\max})$, the threshold corresponding to the maximum value of $D(\Omega_t)$.

3.3 Local Detection Adjustment

For some types of degradation, it may be sometimes more useful to treat the whole image for detecting all the blotches on the image under study. However, this threshold does not

necessarily give the optimum value to detect all blotches accurately. It is therefore necessary to *fine-tune* the threshold for each blotch detected using the global method.
The distortion rate algorithm provides the optimum threshold when calculated on a segment of the image containing only the blotch and image background. When other objects are included in the segment, the threshold tends to rise. The optimum value is taken to be the minimum threshold for that blotch.

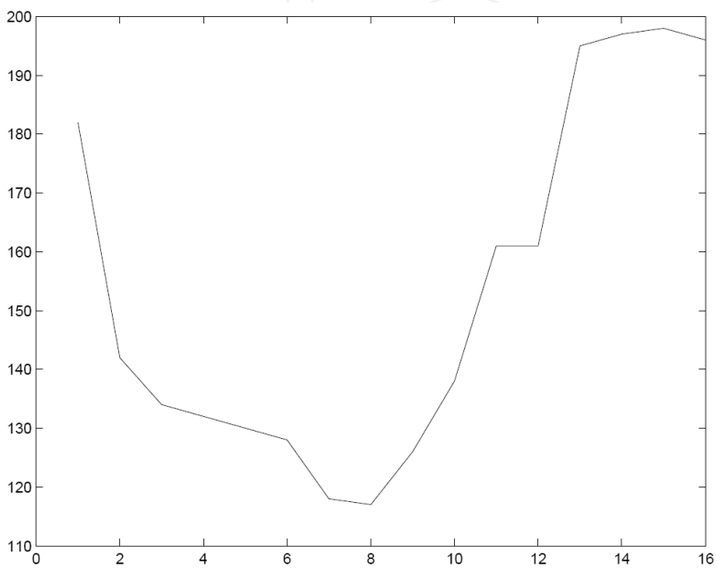

Figure 5. Fine Tuning: A plot of the threshold calculated, $Th(t_{max})$, on a square region around the blotch. As the region grows, the threshold reaches its minimum before increasing again as the region becomes too large

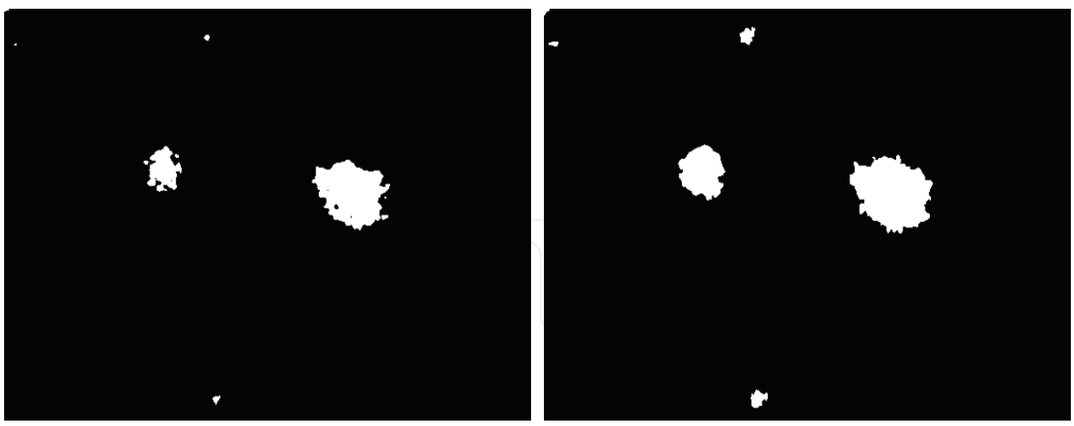

Figure 6. Detection: (Left) Image showing the blotches detected using the global detection algorithm and (Right) final detection mask after local adjustment

In order to find the optimum threshold, each connected region above the global threshold (i.e. each blotch) has its threshold re-evaluated. The Distortion Rate Algorithm is applied repeatedly to square regions around each blotch. Initially, the region is just large enough to contain the previous detection. The detection threshold is calculated for a growing region around the original detection. The threshold changes in agreement with the image content,

increasing whenever new important components of the scene are included in the region. If the thresholds calculated for the increasing region are plotted, it is possible to see that it has a quite convex behaviour (see Fig. 5). More precisely, the curve monotonically decreases till the blotch is almost isolated in regions whose content does not significantly change. Therefore, in practice, the detection algorithm is applied to increasing regions surrounding the botch until the threshold reaches the local minimum. The minimum threshold calculated is taken as the optimum value. The size of the analysed regions increases along both the horizontal and vertical direction according to the optimal resolution $\bar{r}$. Fig. 6 shows an example of a global mask and a local refined mask.

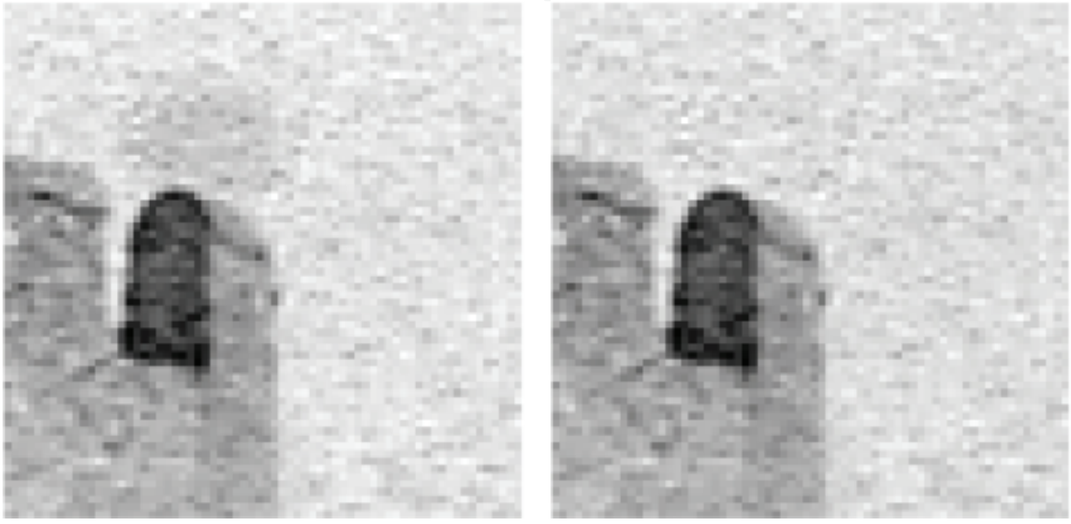

Figure 7. An example of blotch shrinking for achieving restoration: (Left) original, (Right) restored image

4. Perceptive Restoration

Restoration is another delicate step of the whole process. It may seem that after the detection step, restoration may require a minimal effort. On the contrary, it is the most difficult step if the primary objective is to recover the original image without visible artifacts. In order to achieve this goal it is often required, again, a deep knowledge of the physical model of the production of the defect. This usually suggests a possible shape or at least a sort of regularity of the shape of the blotch that should be subtracted from the degraded image. It is worth outlining that this is conceptually different from what generally happens in image processing. In the latter the properties or more specifically the regularity of the original image is assumed as 'a priori' knowledge. For instance, this is the case for denoising (Gonzalez & Woods, 2002; Mallat, 1998). In our case, as already outlined, the original image usually contains details that are still partially visible and that have to be recovered. Since a blotch frequently covers an area with a complicated background, it is not possible to adopt classical schemes for restoration. It is then more opportune a proper shape or regularity of the defect to be attenuated till it is not visible on the degraded image. An example of a restored image is shown in Fig. 7. Moreover, it is also important to highlight the fact that

restoration is not necessarily performed in the same projection space adopted for detection. It often exploits the complementary space as well as different scale levels.

5. Algorithm

Shown below it is a sketch of the algorithm relative to the proposed scheme. The precise definition of the involved operators depends on the case study.

1. Define and perform the projection operator Π on the original RGB image
2. Find the best level of resolution $\bar{r}$ for the projection space, according to Section 3.1
3. Compute the mean value M of $\Pi_{\bar{r}}(I)$
4. Evaluate $D(\Omega_t) \quad \forall Th(t) \geq M$, as defined in Section 3.2
5. Find the maximum point for $D(\Omega_t)$. Let $Th(t_{max})$ be the selected threshold value
6. Produce the global detection mask (see Fig. 6 (left)) as follows:

$$Mask(x,y) = \begin{cases} 1 & if \quad \Pi_{\bar{r}}(I)(x,y) \geq Th(t_{\max}) \\ 0 & otherwise \end{cases}$$

7. Local adjustment performed to give final detection mask B_{mask} (see Fig. 6 (right)).
8. Define a shape or a regularity for the type of blotch under study, accounting for its physical model
9. Shrink the blotch until it is no longer visible — i.e. its contrast in the scene is not perceived

6. First example: scratches on old film

Line scratches are common defects on old film sequences. They appear as straight lines extending over much of the vertical extent of an image frame, as shown in Fig. 8. They can have a different colour and are of a limited width (Kokaram, 1998). They are often caused by mechanical stress during the projection of a film and occupy the same or a similar location in subsequent frames. For this reason, they cannot be classified as temporally impulsive defects.

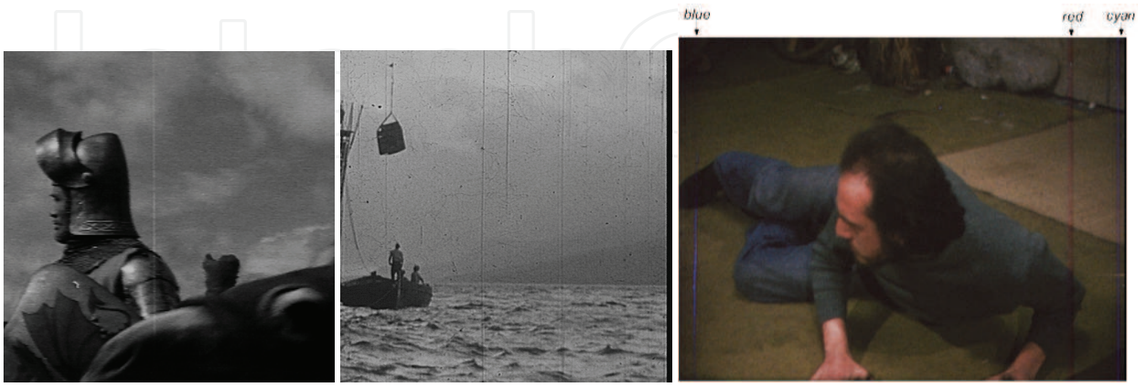

Figure 8. Degraded frames (Knight, Sitdown and Man) having different kinds of scratch, respectively white, black and coloured

The main difficulty in detecting scratches is that they can be confused with other objects of the scene. Conventional detection methods exploit the vertical extension and the impulsive nature of the defect. For example, a suitable combination of the Hough transform for detecting vertical lines and a damped sinusoid model for the scratch horizontal projection is effectively exploited in (Kokaram, 1998), while in (Bretschneider et al., 2000), the scratch is detected in the vertical detail component of a wavelet decomposition, assuming a *sinc* shape for its horizontal projection. On the contrary, in (Joyeux et al. ,1999; Joyeux et al., 2000) scratches are characterized as temporal discontinuities of the degraded image sequence and the Kalman filter is used for their detection. As regards colour scratches, it is worth mentioning the work in (Maddalena & Petrosino, 2005): (intense) blue scratches are detected as maxima points of the horizontal projection of a suitable mask. The latter represents the enhanced vertical lines of the degraded image whose hue, saturation and value amplitudes fall into predefined ranges. With regard to restoration, most of the proposed approaches are based on the assumption that regions affected by scratches do not contain original information (Bertalmio et al., 2000; Bretschneider et al., 2000; Esedoglu & Sheno, 2002; Gulu et al., 2006; Haindl & Filip, 2002; Joyeux et al., 2000; Kokaram, 1998; Rosenthaler & Gschwind, 2001). Hence, they try to propagate neighbouring clean information into the degraded area. The neighbouring information can be found in the same frame (Bertalmio et al., 2000; Bretschneider et al., 2000; Esedoglu & Sheno, 2002; Kokaram, 1998) or also in the preceding and successive frame exploiting the temporal coherency, as done in (Gulu et al., 2006; Haindl & Filip, 2002; Joyeux et al., 2000). The propagation of information can be performed using inpainting methods, as in (Bertalmio et al., 2000; Esedoglu & Sheno, 2002), or interpolation schemes (Kincaid & Cheney, 2002). With regard to this point, different approaches have been presented. In (Kokaram, 1998), an autoregressive filter is used for predicting the original image value within the degraded area. On the other hand, a cubic interpolation is used in (Laccetti et al., 2004), by also taking into account the texture near the degraded area (see also (Rosenthaler et Gschwind, 2001) for a similar approach), while in (Bretschneider et al., 2000) low and high frequency components of the degradation are differently processed. Finally, in (Gulu et al., 2006) each restored pixel is obtained by a linear regression using the block in the image that better matches the neighbourhood of the degraded pixel. A second class of restoration approaches assumes that some of the original information is still contained in the degraded area. For that reason, in (Tenze & Ramponi, 2003) an additive multiplicative model is employed. It consists of a reduction of the image content in the degraded area until it has the same mean and variance of the surrounding information. With regard to blue scratches, in (Maddalena & Petrosino, 2005) removal is performed by comparing the scratch contribution in the blue and green colour channels with the contribution in the red channel; the assumption is that the contribution of scratches in the red channel is negligible.

In the following, after a short explanation of the physical model, a proposal for both detection and restoration is presented.

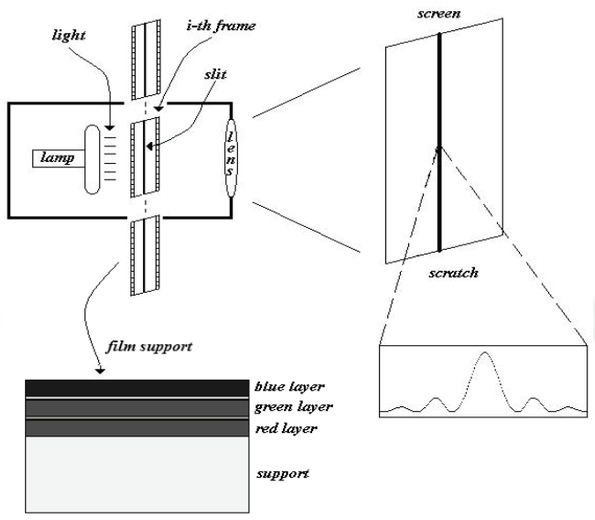

Figure 9. Scheme of the projection mechanism and the structure of the colour film support

6.1 The physical model for line scratches production

Scratches are slits on the film material. They are produced by the film transport mechanism that rubs the film material and removes a part of its content. During the projection or the scanning process, incident light passes through the slit causing diffraction (see Fig. 9). While the width of the slit regulates the width of the observed scratch, the strength (brightness of the observed scratch) of the diffraction effect depends on the depth of the scratch on the film material. In fact, if the projection mechanism does not crack the film, the incident light passes through the residual part of the film material causing the semi-transparency of the observed defect.

Hence, the scratch appears as an area of partially missing data (Bruni & Vitulano, 2004) and the horizontal section of the degraded image I can be modelled as follows

$$I(\bar{x},y) = (1-(1-\gamma)e^{-\frac{2}{m}|y-c_p|})\bar{I}(\bar{x},y) + (1-\gamma)L_{\bar{x}}(y), \quad \forall\ \bar{x} \tag{9}$$

where $\bar{I}$ is the original image, $L_{\bar{x}}(y)$ is the scratch shape function, $2m$ is its width, c_p its location and γ is a normalized parameter to be set according to the visibility of the defect on the whole image. It is tied to the depth of the scratch of the film material: the smaller γ the more perceptible the scratch (i.e. the deeper the slit). From the light diffraction, we have that the horizontal scratch shape is a $\sin c^2$ function (see Fig. 10), i.e.

$$L_{\bar{x}}(y) = b_p \sin c^2\left(\frac{y-c_p}{m}\right), \tag{10}$$

where b_p is the maximum brightness of the scratch on the image. It turns out that the most visible and less transparent part of the degraded region is the central part of the scratch ($y \in R = [c_p - m, c_p + m]$) while the transparency increases for pixels away from the centre.

The mechanical and physical formation of the defect also determines the colour of the observed scratch. In fact, the transport mechanism can impinge either on the side of the support material (negative side) or on the opposite side (positive side). This leads to black

and white scratches respectively, in case of monochromatic frames, or to differently coloured scratches on colour film. In fact, colour film is based on the subtractive synthesis, which filters colours from white light through three separate layers of sensitive (respectively to blue, green and red) emulsions (see Fig. 9). Hence, the colour of the scratch depends on how many (or which) layers have been removed during the stress of the film material.
Finally, not only the width of the slit but also the resolution of the acquisition influences the width of the observed scratch. In case of monochromatic images, this means that scratches can be 3-10 pixels wide, while for colour scratches (resolution 2K, i.e. 1828x1462 pixels) the width can vary from 3 to 30 pixels.

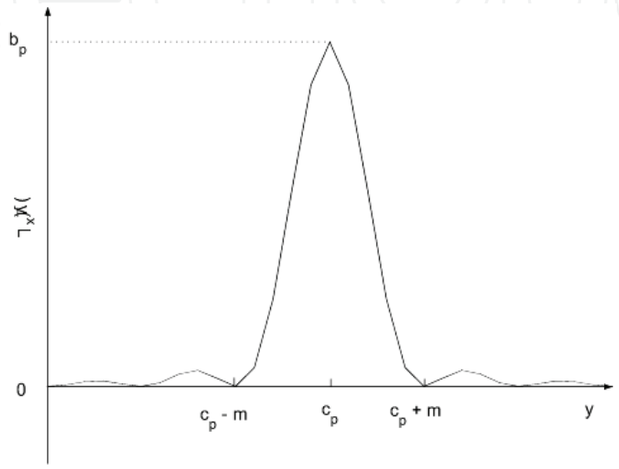

Figure 10. $Sinc^2$ shape of an ideal scratch on the horizontal cross-section of the degraded image, as in eq. (10)

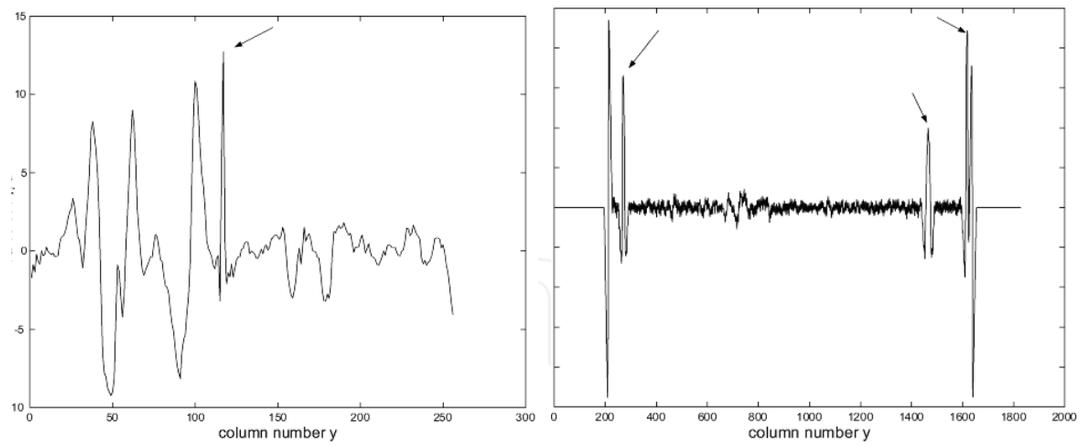

Figure 11. Horizontal cross sections of Knight and Man images in Fig. 8. Scratches are indicated by arrows. Their impulsive nature is evident

6.2. Detection

The main visible property of a scratch is its vertical extension and its horizontal impulsive nature: it is a long and thin line on the image. Hence, the optimal space for processing is that which emphasizes image high vertical frequencies. Moreover, thanks to this property, the detection of this defect can occur in a one dimensional space. Hence, the proper projection

operator Π is the Radon transform of the degraded image I that is computed along the vertical direction, corrected by its local mean. This is the horizontal *cross-section* $\Pi(I)$. Scratches are then peaks of this signal, as show in Fig. 11. In fact, the Radon Transform emphasizes vertical lines while the local mean correction corresponds to a horizontal high pass filter[1].

The optimal scale for perception in this case determines the support of the high pass filter to use in the cross section computation. In our experiments, we observed that optimal scale selection algorithm in Section 3.2 gives $\bar{r} = 10$ for most of all the analysed black and white frames, corresponding to the maximum allowed width for a scratch. The same value has been obtained for colour frames, that have been subsampled by four for computational purposes.

As we have seen, scratches are peaks in the cross section. However, this condition is not sufficient to detect them without introducing false alarms. From the physical model we have some additional information: the observed scratch is caused by diffraction. It turns out that its horizontal shape can be modelled by a $sinc^2$. Hence, the detection algorithm has to extract the visible peaks of $\Pi_{\bar{r}}(I)$ that subtend a $sinc^2$ like shape, whose width is within a prefixed range. In Fig.ure 12 there are the detection results achieved on black and white frames. Scratches are the peaks of $\Pi_{\bar{r}}(I)$ that realize the maximum for the associated distortion in eq. (6). It is worth noticing that in the second picture of Fig.ure 12 the rope has also been detected. In fact, it has the same characteristics of a line scratch and it is highly visible in the image. To reject this kind of false alarms it is necessary to use a more specific procedure along the vertical direction.

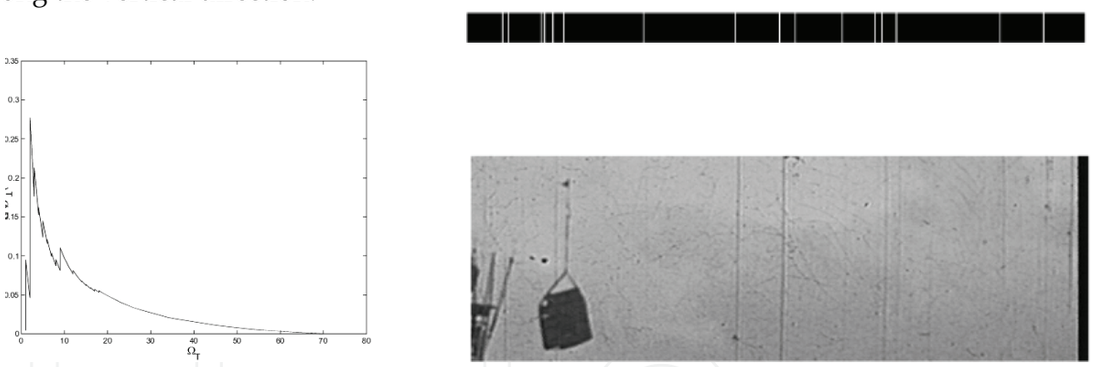

Figure 12. Detection results achieved on Sitdown image in Fig. 8. In the leftmost part of the figure there is the plot of the distortion measure D in eq. (6). The detected scratch locations are indicated in the picture on the right

7. Restoration

As we mentioned in Section 4, the restoration is performed in a domain different from that which is used for the restoration. In this case, we select the wavelet domain where only the low pass component and the vertical details are processed, according to the nature of the defect. The restoration is performed in the wavelet domain using biorthogonal symmetric filters H,G,H_r,G_r in an undecimated decomposition, using the 5/3 taps LeGall filters, as their

[1]In case of colour scratches, the operator Π is applied to the magenta component of the image where scratches are visible as white lines.

width well fits with that of the scratch . H and G respectively are the low pass and high pass analysis filters of the sub-band coding, while H_r and G_r are the corresponding low and high pass synthesis filters. This allows for a better removal of the scratch from the low pass component $I^A(x,y)$ of the degraded image. In fact, the shape of the scratch better fits the data, since it becomes more regular. Then the estimation of the scratch parameters, such as amplitude and width, is less sensitive to the local high frequencies. In the vertical high pass components $I_j^V(x,y)$ of the degraded image, the attenuation corresponds to a reduction of the contrast between the degraded region and the surrounding information at different resolutions, exploiting the semi-transparency model. The maximum level of resolution J for the decomposition is different for each scratch and it depends on its width m. More precisely, $J = \left\lceil \frac{m}{s_H} \right\rceil$, where s_H is the support of the low pass analysis filter H associated with the adopted wavelet. The shrinking coefficients are derived by inverting the equation model (9) and by embedding it in a Wiener filter like function, where the noise is the scratch, i.e.

$$w(\bar{x},y) = \frac{(I^A(\bar{x},y) - c_2 L_{\bar{x}}^A(y))^2}{\left((I^A(\bar{x},y) - c_2 L_{\bar{x}}^A(y))^2 + (\frac{c_2}{c_1} L_{\bar{x}}^A(y))^2\right)}, \quad \forall y \in R \tag{11}$$

where $L_{\bar{x}}^A(y)$ is the low pass component of the function in eq. (10), i.e. $L_{\bar{x}}^A(y) = \sin c^2\left(\frac{y - c_p}{m}\right) * H$, R is the scratch domain, i.e. $R = [c_p - m, c_p + m]$, $c_1 = (1 - (1-\gamma)e^{-\frac{2}{m}|y-c_p|})$, and $c_2 = (1-\gamma)$. Notice that c_1 and c_2 are derived from eq. (9).

The shrinking coefficients $w(\bar{x},y)$ depend on the signal to noise ratio, so that the scratch contribution is attenuated according to its local contrast. In order to make this measure more precise, the algorithm is adapted at each row of the analysed sub-band. In fact, the location c_p of the scratch could slightly change from one row to another, as well as the amplitude b_p and the width m. Therefore, the algorithm firstly corrects the global detection parameters (c_p, b_p, m) according to the local information: location of the maximum, width, asymmetry. In particular, the value of b_p is estimated from the data by minimizing the mean square error in the scratch domain R, i.e.

$$b_p = \min_{\alpha \in R} \sum_{y \in R} \left| I^A(\bar{x},y) - \alpha L_{\bar{x}}^A(y) \right|^2 \tag{12}$$

b_p is then the peak value of the $sinc^2$ function that better matches, in the least squares sense, with the data at the considered resolution. The same procedure is repeated for the vertical detail bands $I_j^V(x,y)$ at scale j=1,…,J.

Some examples of restored images are depicted in Fig. 13. As it can be observed the visual quality of the restored image is satisfying. Scratches are removed without introducing blurring or artifacts both in the image content and in colour information, independently of the context. In particular, the underlying original information, texture or noise, is preserved

thanks to the adaptivity of the attenuation filter in eq. (11) to the local image content, inside and outside the degraded region, even in presence of a diagonal edges — see the shoulder in the Knight figure, the see in Sitdown or the carpet in Man image. A Zoom of Man image is also depicted in Fig. 14.

Figure 13. Restored frames in Fig. 8 using the proposed algorithm

Figure 14. Zoom of the red scratch of Man frame in Fig. 8 (*left*) restored using the proposed algorithm (*right)*

8. Second example: water blotches on archive documents

The second example focuses on water blotches that are probably the most common defect on archived documents (Stanco et al., 2003; Bruni et al., 2004; Stanco et al., 2005). Such blotches are caused by water penetration into paper whose effect is a darker region on the document with variable shape, colour and intensity. Occasionally, dirt and dust are also present: This alters and complicates the blotch's structure.

Although an immediate detection by the human visual system on very complicated contexts, both digital detection and restoration are very difficult. Detection is difficult as the semi-transparent nature of the blotch leaves almost all high frequency information unchanged — see for instance (Bruni et al., 2006; Ramponi et al., 2005). But also the restoration phase is not trivial at all. In fact, for historical reasons the objective is to recover the document information as much as possible so that classical methods, those which synthesize information, cannot be used (Beltarmio et al, 2000; Beltarmio et al., 2003; Criminisi, 2004; Gonzalez & Woods, 2002; Kokaram, 2001). In order to reduce restoration costs, an automatic model that simulates the efficacy of the human visual system is required. In the following, after a short explanation of the physical model that causes their formation, a proposal for both detection and restoration is presented.

8.1 The physical model for water blotch production

The physical formation of a water blotch can be modelled by the spreading and penetration of water droplets into material (Clarke et al., 2002; Seveno et al., 2002). The evolution of a drop involves different parameters, such as the geometry of the original drop and the regularity of the surface of the paper. However, these parameters are unknown in real applications. The problem can be simplified by modelling the water drop as a semi-sphere (see Fig. 15) of radius R with a contact angle θ, assumed to be $\leq \pi/2$. During the spreading process, the radius grows to an equilibrium point which determines the contact angle. From this point on, the liquid is absorbed depending on the porosity of the considered medium. In ideal conditions, the central pores absorb more than the external pores, since they come in contact with the liquid earlier. This can be seen in most blotches, where the effects of the blotch are most evident towards its centre. In most cases, the spreading and absorption

processes have been completed so that there is a small contact angle i.e. a smooth transition to the unaffected area.

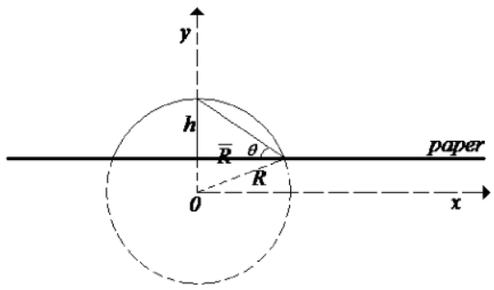

Figure 15. Model of a water drop's absorption into paper, causing a blotch

8.2 Detection

The detection phase has been performed on the Pyramid image shown in Fig. 2. left. Water blotches can be characterized by both a blurring of the degraded region and, typically, a redder colour — even though its intensity may change considerably. Hence, both the saturation component of the HSV space (that emphasizes the blurring) or an alternative component that emphasizes the redder regions can be employed. Here, the following component is proposed:

$$\Pi(I)(x,y) = Y(x,y) - Blue(x,y) \tag{13}$$

where

$$Y(x,y) = 0.3\ Red(x,y)+0.59\ Greeen(x,y)+0.11\ Blue(x,y) \tag{14}$$

and *Red*, *Green* and *Blue* are the colour channels in the RGB colour space.

Figure 16. (Left) Blotches appear as bright regions in the selected projection space $\Pi(I)$, as in eq. (13). (Right) Its smoothed version at scale level J=2

Fig. 16.Left shows the blue difference image $\Pi(I)$, based on contrast caused by opposed proportions of colours. In order to apply eq. (3) to select the optimal resolution, a suitable filter has to be employed. Here, the physical model plays a key role. In fact, the value of $\bar{r}$

reached via this process can be linked to a scale level J in a pyramidal decomposition (for instance a dyadic wavelet decomposition): $J = \log_2 \left\lfloor \frac{\bar{r}}{s_H} \right\rfloor$, where s_H is the length of the low pass filter associated to the adopted wavelet. The *db2* (Daubechies with two vanishing moments (Mallat, 1998)) mother wavelet has been adopted as it has both minimum support and a reasonable regularity that are well adapted to the characteristic of the defect — blotches can also be regions containing 2 or 3 pixels. The computed scale level (in an undecimated dyadic decomposition) is the second one, i.e. J=2. The resulting image is shown in Fig. 16.Right.

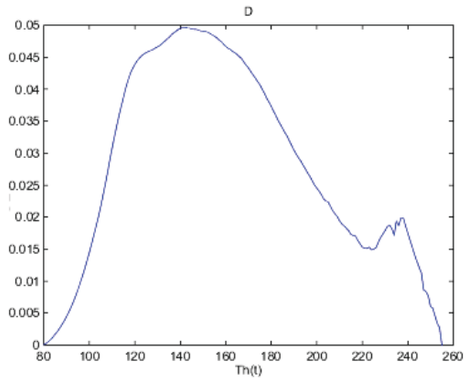

Figure 17. Distortion curve on the Pyramid image

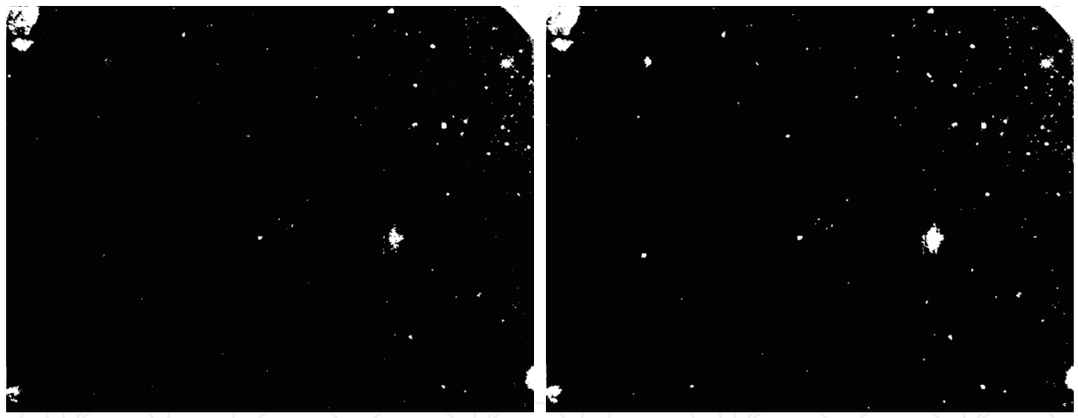

Figure 18. (Left) Mask achieved by a global threshold. (Right) Mask after the local refinement

Figure 19. (Left) Original detail of Pyramid image. (Middle) Projection space image. (Right) Resulting final mask

At this point, the distortion introduced in section 3.2 can be performed. The plot of the distortion behaviour is shown in Fig. 17. The global detection mask, that is the output output of this phase is depicted in Fig. 18.Left. It can be observed that all blotches are automatically detected. However, if a more accurate localization is required, a local refinement has to be performed. The result of this operation is shown in Fig. 18. Right where it can be seen that blotch mask has been refined by filling holes or dilating smaller blotches. A zoom showing a small part of the sky and the castle with the relative mask is shown in Fig. 19.

8.3 Restoration

The restoration process can be performed as follows. The original (sepia) image is transformed to the HSV colour space. Each of the H (hue), S (saturation) and V (value) components are split into an over-complete wavelet basis until the optimal scale level, J. The approximation band of the intensity component V^A is restored according to the transparency model and perception laws yielding $\widetilde{V}^A$. The wavelet details of the same colour component $\{V_j^D\}_{1\le j\le J}$ are left unchanged since such kind of blotch very often are smooth in agreement with the aforementioned physical model[2]. Finally, the inverse wavelet transform is performed to achieve $\widetilde{V}$. The chroma components approximations H^A and S^A are subsequently processed yielding $\widetilde{H}$ and $\widetilde{S}$ after the inverse wavelet transform. The final restored image $\hat{I}$ is given when $\widetilde{H}$, $\widetilde{S}$ and $\widetilde{V}$ are transformed in an RGB image.

As the blotch does not completely obscure the clean image, the luminance approximation band can be modelled as a multi-layer image similar to (Wang & Adelson, 1994), i.e. the luminance approximation band is modelled as a mixture between the clean image layer and the blotch layer (White et al., 2005). The layers mix is based on the following relationship:

$$V^A(\mathbf{x}) = \alpha(\mathbf{x})\widetilde{V}^A(\mathbf{x}) + \varepsilon(\mathbf{x}) \tag{15}$$

where $V^A(\mathbf{x})$ is the observed luminance approximation band at point $\mathbf{x}$, $\alpha(\mathbf{x})$ the distortion layer and $\widetilde{V}^A(\mathbf{x})$ the clean luminance approximation band. Noise is represented by $\varepsilon(\mathbf{x}) \sim N(0, \sigma_\varepsilon^2)$. Therefore, the restored luminance approximation will be:

$$\widetilde{V}^A(\mathbf{x}) = V^A(\mathbf{x})\beta(\mathbf{x}) \tag{16}$$

where $\beta(\mathbf{x})$, the restoration function, equals: $\beta(\mathbf{x}) = (\alpha(\mathbf{x}))^{-1}$.

The correct values of $\widetilde{V}^A$ and α are those which maximise $p(\widetilde{V}^A, \alpha \mid V^A, \sigma_\varepsilon^2)$. Bayes' law gives the following relationship

$$p(\widetilde{V}^A, \alpha \mid V^A, \sigma_\varepsilon^2) \propto p(V^A \mid \widetilde{V}^A, \alpha, \sigma_\varepsilon^2) p(\alpha \mid \overline{\alpha}) p(\widetilde{V}^A \mid \overline{\widetilde{V}^A}) \tag{17}$$

where $\overline{\alpha}$ and $\overline{\widetilde{V}^A}$ are α and $\widetilde{V}^A$ in the neighbourhood of $\mathbf{x}$ respectively. It is now easier to compute the likelihoods on the right hand side of the previous equation in place of

[2]Cases where dirt causes a visible borderline of the blotch are not considered here.

$p(\widetilde{V}^A, \alpha \mid V^A, \sigma_\varepsilon^2)$. The first two likelihoods on the right hand side ensure that alpha matches the behaviour of the blotch described, i.e. *i)* α must mix to give the observed data; *ii)* α must be smooth. The third term ensures that $\widetilde{V}^A$ values are similar. The probabilities from expression (17) can be represented as follows:

$$p(V^A \mid \widetilde{V}^A, \alpha, \sigma_\varepsilon^2) \propto \exp\left(\frac{-\left(V^A(x) - \alpha(x)\widetilde{V}^A(x)\right)^2}{2\sigma_\varepsilon^2} \right) \tag{18}$$

$$p(\alpha \mid \overline{\alpha}) \propto \exp\left(-\sum_{k=0}^{n} \lambda_k (\alpha(x) - \alpha(x+q_k))^2 \right) \tag{19}$$

$$p(\widetilde{V}^A \mid \overline{\widetilde{V}^A}) \propto \exp\left(-\sum_{k=0}^{n} \lambda_k (\widetilde{V}^A(x) - \widetilde{V}^A(x+q_k))^2 \right) \tag{20}$$

where $\mathbf{x} + q_k$ is a neighbouring sample and λ_k is a weight based the distance to this sample. These expressions show that maximising $p(\widetilde{V}^A, \alpha \mid V^A, \sigma_\varepsilon^2)$ is equivalent to minimising the following energy:

$$E = W_1 \frac{-\left(V^A(x) - \alpha(x)\widetilde{V}^A(x)\right)^2}{2\sigma_\varepsilon^2} + W_2 \sum_{k=0}^{n} \lambda_k (\alpha(x) - \alpha(x+q_k))^2 + W_3 \sum_{k=0}^{n} \lambda_k (\widetilde{V}^A(x) - \widetilde{V}^A(x+q_k))^2 \tag{21}$$

Weights W_1, W_2 and W_3 regulate the emphasis on the different constraints modelled by the three terms of (21).

With regard to the algorithm, there are two main steps in the restoration process. The first step initialises each pixel inside the blotch. To each pixel is assigned a value chosen from the "clean" area close to the pixel. The next step uses the Iterative Conditional Mode (ICM) algorithm (Besag, 1986) to minimise the energy *E* from equation (21). The resulting images from these steps are shown in Fig. 20.

The initialisation step is a simple image synthesis method. For each pixel, its value is taken as a sample drawn from local "clean" pixels similar to the method used in (White et al., 2005). The local region is composed of all clean pixels contained within a circle, centred on the current pixel. The radius of the circle is proportional to the distance between the pixel and the nearest edge of the blotch. Specifically the radius is defined as: $\log(d(x)+1)+s_{\psi J}$ where $d(\mathbf{x})$ is the distance to the edge and $s_{\psi J}$ is the wavelet support at the considered scale level *J*. The initialisation provides a reasonable solution for the blotch. However, it is void of the original underlying information clearly visible in the original image due to the semi-transparent properties of the blotch. To recover this information, *E* must be minimised using the original image. The initialisation gives the initial conditions for the minimisation process, $\widetilde{V}_0^A$ and α_0. The minimisation is carried out using the ICM algorithm recursively improving estimates for $\widetilde{V}_0^A$ and α as follows:

$$\widetilde{V}_1^A \approx p(\widetilde{V}^A \mid V^A, \alpha_0, \sigma_\varepsilon^2) \quad \alpha_1 \approx p(\alpha \mid V^A, \widetilde{V}_1^A, \sigma_\varepsilon^2), \quad \widetilde{V}_2^A \approx p(\widetilde{V}^A \mid V^A, \alpha_1, \sigma_\varepsilon^2) \quad \alpha_2 \approx \ldots,$$

In practice, the value of α is fixed, and the E is calculated for a large range of $\tilde{V}^A$ ([0,0.01,-0.02,0.03,…,0.99,1] for a normalised image). $\tilde{V}^A$ is selected as that which gives the minimum value of E. The process is repeated fixing $\tilde{V}^A$ and calculating E for a range of α. This is repeated until the whole blotch converges, i.e. the restored approximation band $\tilde{V}^A$ is reached. The blotch is processed from the outside-in on the premise that values drawn from closer neighbourhoods are more likely to be accurate.

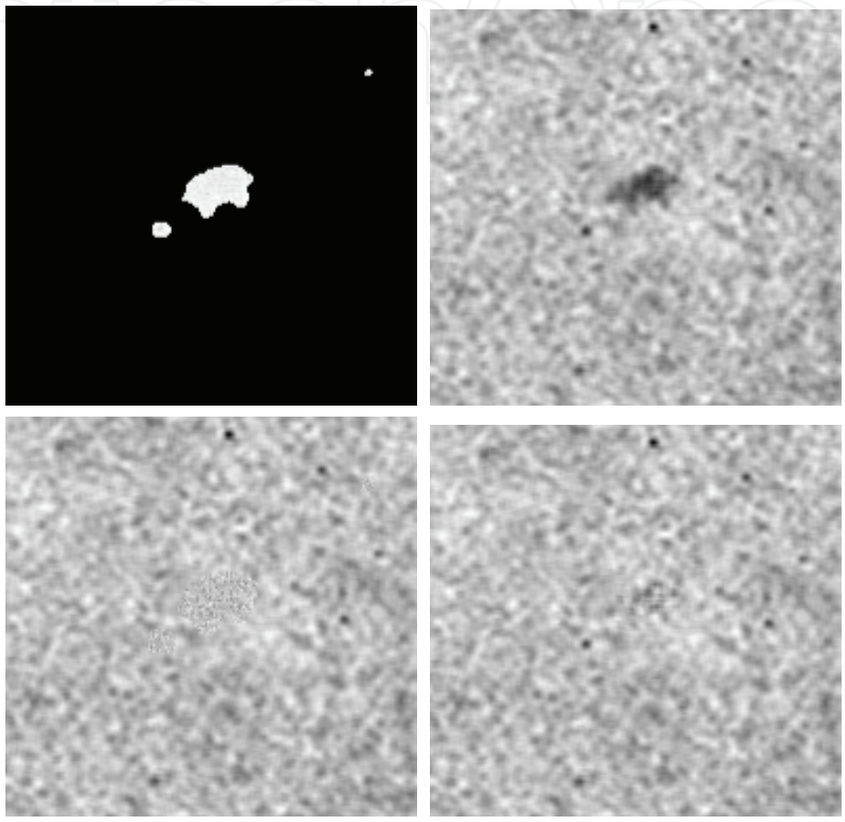

Figure 20. Luminance Restoration: The approximation (topright) is first initialised (bottomleft) and then the minimisation is carried out (bottomright)

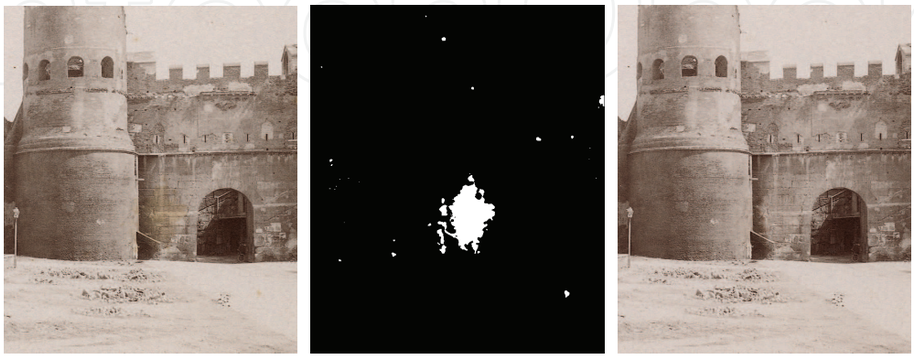

Figure 21. Blotch Restoration: Wall section of the Pyramid image restored using the proposed method (Original image, Blotch Mask and Restored Image)

Although colour images are being processed, the clean image is almost constant in colour. In the areas affected by the blotch, Hue and Saturation values are increased. However, there is no underlying colour detail as in the luminance channel. Therefore, the simple texture synthesis method adopted as the initialisation for the luminance process, applied to the approximations of H and S, is sufficient to remove the effects of the blotches from the chroma channels H and S. Finally, the restored H, S and V channels are combined to give the final restored RGB image. In order to better appreciate the proposed scheme on this kind of blotches, Figs. 21, 22, 23, show the intermediate steps as well as the final result on a zoom of the Pyramid image.

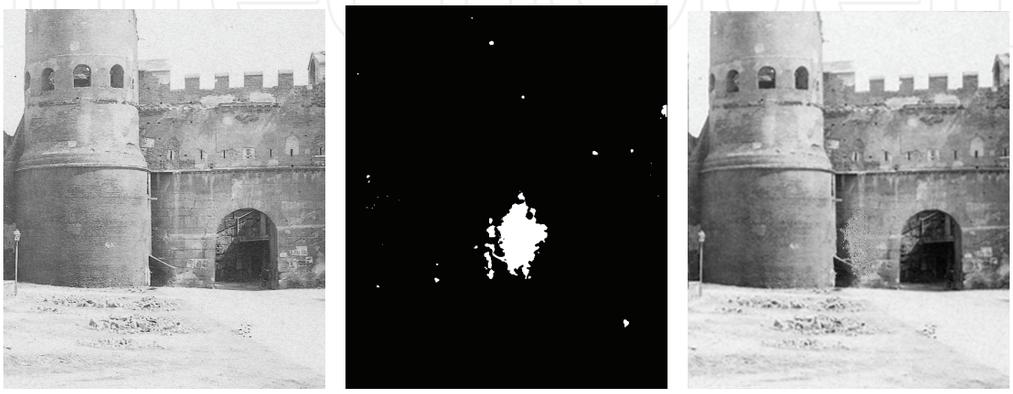

Original Luminance | Luminance Approximation | Initialisation

Minimisation | Alpha Function | Restored Luminance

Figure 22. Luminance Restoration: The four steps in Luminance restoration. Firstly, the wavelet approximation is calculated. The degraded regions are then initialised and minimisation is carried out. The Wavelet Transform is then inverted to give the restored Luminance

9. Conclusion

The two examples above show that the use of human visual perception can help in various fields of image processing and in particular in image restoration. Even though the model and the corresponding framework presented in this paper are just a first step in this direction, the achieved results show the huge potentiality of this approach. There are many cases, like those presented, that classical tools of image processing cannot manage in an

efficacious manner. This is true both from the quality and from the automaticity point of view. In particular, visibility based techniques become a need for semitransparent blotches restoration. The examples of this contribution have been selected in order to present a case where image restoration shows its limits because of the difficulty in discerning the original information from the degradation one. Moreover, in cases like the aforementioned one, the line between a low level (strictly tied to the human visual system) and a high level perception (where also the brain with its classification functions is involved) becomes very subtle. We hope that this work can be a stimulus for a greater effort in investigating this interesting topic.

10. Acknowledgements

This paper has been partially supported by the FIRB project no.RBNE039LLC, "A knowledge-based model for digital restoration and enhancement of images concerning archaeological and monumental heritage of the Mediterranean coast".
The authors would like to thank Fratelli Alinari S.p.A and the Sacher Film s.r.l. for providing all the pictures and frames used in this paper.

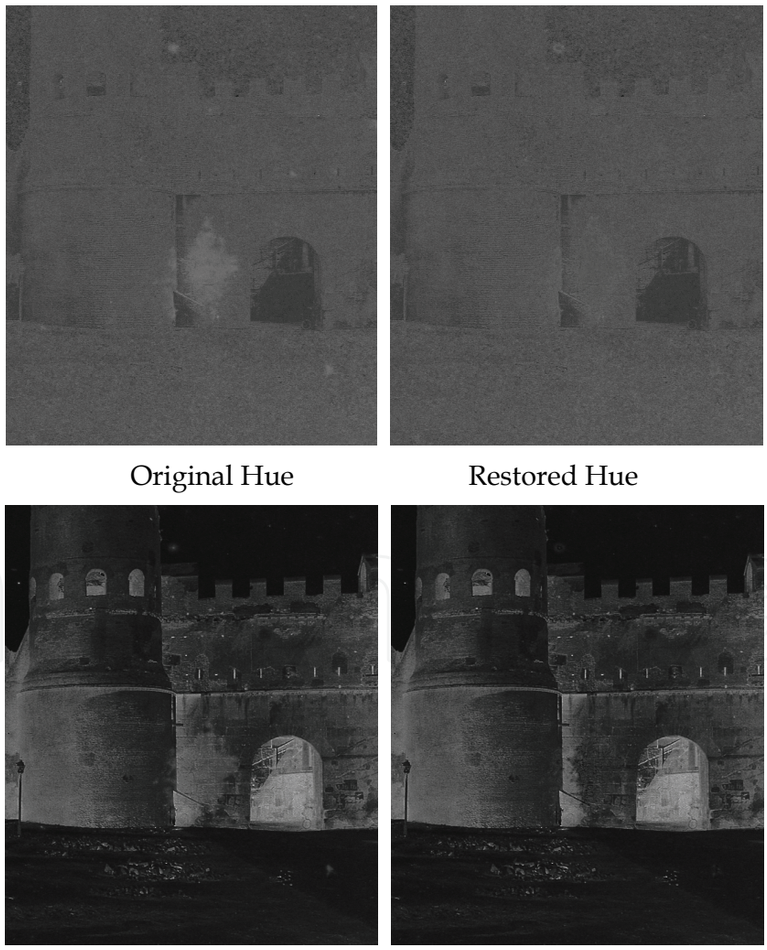

Original Hue Restored Hue

Original Saturation Restored Saturation

Figure 23. Degraded Hue and Saturation along with their restored version

11. References

Barba, M. & Barba, D. (2002). Simulating the human visual system: towards objective measurement of visual annoyance. *IEEE Transactions on Systems, Man and Cybernetics*, vol. 6, October 2002

Beltarmio, M.; Vese, L.; Sapiro, G.; Caselles, V. & Osher, S. (2003). Simultaneous structure and texture image inpainting. *IEEE Transactions on Image Processing*, vol. 12, August 2003, pp. 882 –889

Beltarmio, M; Sapiro, G.; Caselles, V. & Ballester, C. (2000). Image inpainting. *Computer Graphics, SIGGRAPH 2000*, July 2000

Besag, J. R. (1986). On the analysis of dirty pictures. *Journal of the Royal Statistical Society B*, vol. 48, pp. 259–302

Bretschneider, T.; Kao, O. & Bones, P.J. (2000). Removal of vertical scratches in digitised historical film sequences using wavelet decomposition. *Proc. of Image and Vision Computing New Zealand*, 2000, pp. 38–43

Bruni, V.; Crawford, A.; Stanco, F. & Vitulano, D. (2006) . Visibility based detection and removal of semi-transparent blotches on archived documents. *Proc. of Int. Conf. on Computer Vision Theory and Applications (VISAPP)*, Setùbal, Portugal, February 2006

Bruni, V. & Vitulano, D. (2004). A generalized model for scratch detection. *IEEE Transactions on Image Processing*, vol. 13, no. 1, January 2004, pp. 44 – 50

Clarke, A.; Blake, T.D.; Carruthers, K. & Woodward, A.(2002) . Spreading and imbibition of liquid droplets on porous surfaces. *Langmuir Letters 2002 American Chemical Society*, vol. 18, no. 8, pp. 2980–2984

Corrigan, D. & Kokaram, A. (2004). Automatic treatment of film tear in degraded archived media. *Proc. of Int. Conf. Image Processing (ICIP '04)*, Singapore, October 2004

Criminisi, A.; Perez, P. & Toyama, K. (2004). Region filling and object removal by exemplar-based image inpainting. *IEEE Transactions on Image Processing*, vol. 13, no. 9, September. 2004, pp. 1200–1212

Damera-Venkata, N.; Kite, T. D.; Evans B. L. & Bovik, A. C.(2000). Image quality assessment based on a degradation model. *IEEE Trans. on Image Processing*, vol. 9, no.4, April 2000, pp. 636–650

Esedoglu, S. & Sheno, J.. (2002). Digital inpainting based on the mumford-shah-euler image model. *European J. Appl. Math*, vol. 13, pp. 353–370.

Gonzalez, R. C. & Woods, R. E. (2002) *Digital Image Processing*. Prentice Hall, 2nd edition

Gulu, M.K. ; Urhan, O. & Erturk, S. (2006). Scratch detection via temporal coherency analysis and removal using edge priority based interpolation. *Proc. of IEEE International Symposium on Circuits and Systems, 2006*, May 2006.

Gutiérrez, J. ; Ferri, F. J. & Malo, J. (2006). Regularization operators for natural images based on nonlinear perception models. *IEEE Transactions on Image Processing*, vol. 15, no. 1, January 2006, pp. 189–200.

Haindl, M. & Filip, F. (2002). Fast restoration of colour movie scratches. *Proc. of ICPR 2002, Quebec, Canada*, August 2002, pp. 269–272.

Joyeux, L. ; Boukir, S. &Besserer, B. (2000). Film line removal using kalman filtering and bayesian restoration. *Proc. of IEEE WACV'2000, Palm Springs, California*, December 2000.

Joyeux, L. ; Buisson, O. ; Besserer, B.& Boukir, S.(1999). Detection and removal of line scratches in motion picture films. *Proc. of CVPR'99, Fort Collins, Colorado, USA*, June 1999.

Kincaid, D. & Cheney, W.(2002). *Numerical analysis*. Brooks/Cole, 2002.

Kokaram, A. C. (2001). Advances in the detection and reconstruction of blotches in archived film and video. *Proceedings of the IEE Seminar on Digital Restoration of Film and Video Archives*, London UK, January 2001.

Kokaram, A.C. (2004). On missing data treatment for degraded video and film archives: a survey and a new bayesian approach. *IEEE Transactions on Image Processing*, vol. 13, no. 3, March 2004, pp. 397 – 415.

Kokaram, A.C. (1998) *Motion Picture Restoration: Digital Algorithms for Artefact Suppression in Degraded Motion Picture Film and Video*. Springer Verlag

Laccetti, G. ; Maddalena, L. & Petrosino, A. (2004). Parallel/distributed film line scratch restoration by fusion techniques. *Lectures Notes in computer Science, Springer Berlin*, vol. 3044/2004, September 2004, pp. 525–535.

Maddalena, L. & Petrosino, A. (2005). Restoration of blue scratches in digital image sequences. *Technical Report ICAR-NA*, vol. 21, December 2005.

Mallat, S. (1998) *A Wavelet Tour of Signal Processing*. Academic Press

Nadenau, M. J.; Reichel, J. & Kunt, M. (2003) Wavelet-based color image compression: Exploiting the contrast sensitivity function. *IEEE Transactions on Image Processing*, vol. 12, no. 1, January 2003, pp. 58–70.

Pappas, T.N. & Safranek, R.J.(2000). Perceptual criteria for image quality evaluation. *Handbook of Image and Video Processing (A. C. Bovik, ed.)*, Academic Press 2000, pp. 669–684.

Peli, E. (1990). Contrast in complex images. *Journal of the Optical Society of America A*, vol. 7, October 1990, pp. 2032–2040.

Ramponi, G. ; Stanco, F. ; Dello Russo, W. ; Pelusi, S. & Mauro, P. (2005). Digital automated restoration of manuscripts and antique printed books. *Proc. of Electronic Imaging and the Visual Arts (EVA)*, Florence, Italy, March 2005.

Rosenthaler, L. & Gschwind, R. (2001). Restoration of movie films by digital image processing. *Proc. of IEE Seminar on Digital Restoration of Film and Video Archives 2001*, 2001.

Seveno, D.; Ledauphine, V.; Martic, G. & Voué, M. (2002). Spreading drop dynamics on porous surfaces. *Langmuir 2002 American Chemical Society*, vol. 18, no. 20, pp. 7496–7502.

Stanco,F., Ramponi, G. & De Polo, A.(2003). Towards the automated restoration of old photographic prints: A survey. In *IEEE EUROCON*, Ljubjana, Slovenia, Sept. 2003, pp. 370–374.

Stanco, F.; Tenze, L. & Ramponi, G. (2005). Virtual restoration of vintage photographic prints affected by foxing and water blotches. *Journal of Electronic Imaging*, vol 14, no. 4, December 2005.

Tenze, L. & Ramponi, G. (2003). Line scratch removal in vintage film based on an additive/multiplicative model. *Proc. of IEEE-EURASIP NSIP-03, Grado, Italy*, June 2003.

van Roosmalen, P.M.B.; Lagendijk, R.L. & Biemond, J. (1999). Correction of intensity flicker in old film sequences. *IEEE Transactions on Circuits and Systems for Video Technology*, vol. 9, no. 7, pp. 1013–1019.

Wang J.Y. A. & Adelson, E. H. (1994). Representing moving images with layers. *IEEE Transactions on Image Processing*, vol. 3, no. 5, September 1994, pp. 625–638.

White, P.R. ; Collis, W.B.; Robinson, S. & Kokaram, A.C. (2005). Inference matting. *Proc. of Conference on Visual Media Production (CVMP)*, November 2005.

Winkler, S. (2005) *Digital Video Quality - Vision Models and Metrics*. John Wiley and Sons

Brain, Vision and AI

Edited by Cesare Rossi

ISBN 978-953-7619-04-6

Hard cover, 284 pages

Publisher InTech

Published online 01, August, 2008

Published in print edition August, 2008

The aim of this book is to provide new ideas, original results and practical experiences regarding service robotics. This book provides only a small example of this research activity, but it covers a great deal of what has been done in the field recently. Furthermore, it works as a valuable resource for researchers interested in this field.

How to reference

In order to correctly reference this scholarly work, feel free to copy and paste the following:

V. Bruni, A. J. Crawford, A. Kokaram and D. Vitulano (2008). Visual Perception of Semi-transparent Blotches: Detection and Restoration, Brain, Vision and AI, Cesare Rossi (Ed.), ISBN: 978-953-7619-04-6, InTech, Available from: http://www.intechopen.com/books/brain_vision_and_ai/visual_perception_of_semi-transparent_blotches__detection_and_restoration

INTECH

open science | open minds

InTech Europe

University Campus STeP Ri
Slavka Krautzeka 83/A
51000 Rijeka, Croatia
Phone: +385 (51) 770 447
Fax: +385 (51) 686 166
www.intechopen.com

InTech China

Unit 405, Office Block, Hotel Equatorial Shanghai
No.65, Yan An Road (West), Shanghai, 200040, China
中国上海市延安西路65号上海国际贵都大饭店办公楼405单元
Phone: +86-21-62489820
Fax: +86-21-62489821

IntechOpen